Available online at www.sciencedirect.com
ScienceDirect
Journal of Power Sources 161 (2006) 474–483
JOURNAL OF POWER SOURCES
www.elsevier.com/locate/jpowsour

Performance of alkaline fuel cells: A possible future energy system?

Betty Y.S. Lin [a,*], Donald W. Kirk [b], Steven J. Thorpe [a]

[a] *University of Toronto, Department of Materials Science and Engineering, 184 College Street W., Toronto, Ont., Canada M5S 3E4*
[b] *University of Toronto, Department of Chemical Engineering, 200 College Street W., Toronto, Ont., Canada*

Received 21 October 2005; received in revised form 10 March 2006; accepted 28 March 2006
Available online 5 May 2006

Abstract

Alkaline fuel cells (AFCs) are amongst the most mature fuel cell technologies having been in use since the mid 1960s by NASA in the Apollo and Space Shuttle programs. The AFC process is revisited to define current operating characteristics as the baseline for future developments of AFC technologies that can take advantage of advances in alkaline water electrolysers (AWEs). The end purpose is to advance a design that connects and shares as many peripherals in an AFC with that of an AWE.

Good AFC performance can be achieved by keeping the operating temperature below 70 °C in order to avoid cell damage, the electrolyte concentration should be kept ∼8 M to obtain optimum ionic conductivity, and excess gas is needed for the fuel cell to start and display stable operation. In order to understand the link of degradation in cell performance with the materials used in the construction of the fuel cell, the catalytic layer of both the anode and cathode was analyzed. Results showed that improvement in electrochemical performance could be achieved by better catalyst chemistry, structural form and distribution.

Keywords: Alkaline fuel cell performance; Alkaline fuel cell electrode degradation

1. Introduction

Alkaline fuel cells (AFCs) are amongst the most mature fuel cell technologies having been in use since the mid 1960s by NASA in the Apollo and Space Shuttle programs [1–3]. The fuel cells on these spacecrafts provide electrical power for on-board systems, as well as drinking water. Advanced AFCs have the highest electrical efficiency (at nearly 70%) in generating electricity and have shown excellent reliability when run at low current densities. AFCs are able to use non-noble catalysts, thereby significantly reducing the capital cost of the stack. By using a circulating electrolyte, good internal thermal management is readily achieved. AFCs can operate on air (scrubbed of CO_2), and they have fast oxygen kinetics under basic electrolyte conditions. AFCs have lost their popularity to other new emerging fuel cell technologies such as proton exchange membrane fuel cells (PEMFC) for vehicular applications because of the flexibility of using a solid electrolyte and concerns of electrolyte leakage.

Over the past decade, significant developments have been made in the parallel field of Alkaline Water Electrolysis (AWE). AWE has high current efficiencies of up to 99%, and yield high gas purities of >99.9% for hydrogen, and 99.5% for oxygen in high temperature and pressure operation using advanced materials for frames, seals and electrode structures. In this paper, the AFC process is revisited to define current operating characteristics as the baseline for future developments of AFC technologies that can take advantage of advances in AWEs. The end purpose is to advance a systems approach to a design that connects and shares as many balance of plant peripherals in an AFC with that of an AWE to significantly lower the overall system cost compared with independent devices. It was found that although there are many advantages to the AFC, there are also challenges that need to be overcome in order to advance the AFC technology to the same level as the AWE.

AFCs have evolved throughout the years. Better electrode materials have allowed for lighter and thinner electrodes. Operating temperature and pressure also decrease with time, along with the amount of noble catalyst loadings. Matrix-type electrolytes are still used for space applications to produce high power.

* Corresponding author. Tel.: +1 416 978 8573; fax: +1 416 978 4155.
E-mail address: betty.lin@utoronto.ca (B.Y.S. Lin).

0378-7753/$ – see front matter © 2006 Elsevier B.V. All rights reserved.
doi:10.1016/j.jpowsour.2006.03.052

Today, AFCs are targeted for possible incorporation in small off-road vehicular applications such as golf carts, forklifts, stationary applications to power cottages, residential homes, and back-up power for offices, hospitals, businesses and houses. Such application requires a reconsideration of the liquid electrolyte units for the many advantages that the circulating electrolyte offers. The R&D required includes a reliable barrier against reactant leakage from the electrodes and the use of the electrolyte as a cleansing medium, for removal of impurities such as carbonates, and heat and water generated within the fuel cell.

To fully understand the operating parameters of an alkaline fuel cell through experimentation, the operating characteristics of an AFC were determined by measuring the effect of operating temperature, electrolyte concentration, and gas flow rates on the AFC performance (current and voltage). The degradation of electrodes in an alkaline fuel cell were investigated in order to understand the link between degradation in cell performance and the materials used in the construction of the fuel cell, the catalytic layer of both the anode and cathode were analyzed. Improvement in electrochemical performance will also be discussed.

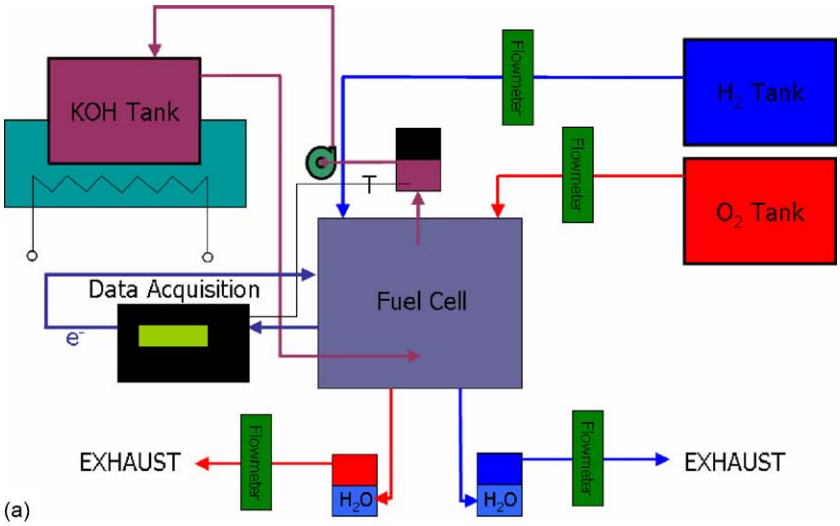

(a)

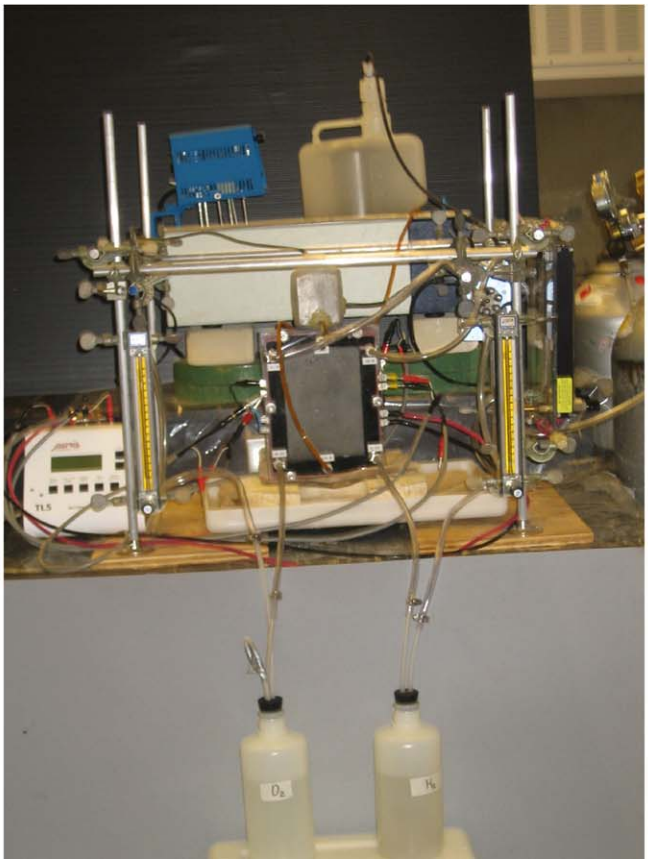

(b)

Fig. 1. (a) Process flow diagram of experimental set-up: AFC with inputs and outputs. (b) Actual diagram of experimental set-up: AFC with inputs and outputs.

2. Experimental

The AFC that was tested contained 4 cells connected in series to form one stack. The edge-collected cells have tabs at the edges of the electrodes to connect one electrode to another. A single cell may be disconnected in case of failure without seriously disturbing the performance of the other cells.

The dimensions of the stack are nominally 23 cm × 18 cm × 6 cm. Each electrode contained an active area of 200 cm^2. An 8 M potassium hydroxide (KOH) electrolyte was used. The gases used in the experiments were taken directly from H_2 and O_2 gas tanks with purities 99.999% and 99.6%, respectively, and fed at pressures close to atmospheric.

There are three main loops in the process flow: electrolyte, gases, and electrons. The fuel cell operates at <1 psi (<6.9 kPa) backpressure. Fig. 1a and b shows the process flow diagram, and the actual experimental apparatus.

KOH was prepared by mixing 448.8 g of VWR KOH Analar^{TM} grade pellets to 830 mL of ASTM Type I water to make 1 L of solution. The KOH electrolyte stored in a reservoir and was heated in a water bath by using a circulator or heating coil to 70 °C. The electrolyte was gravitationally fed into the bottom of the fuel cell, where it fills the cell and exits through the top of the fuel cell into a small overflow chamber creating a back pressure of <1 psi (<6.9 kPa). The electrolyte is then pumped back into the reservoir via a peristaltic pump recirculating the electrolyte throughout the entire experiment.

The electrodes were preconditioned by immersion in the electrolyte for an hour. Then, H_2 and O_2 gases were fed into the AFC from gas tanks. The gas pressure and flowrates are controlled by a regulators and flowmeters, respectively. Hydrogen/oxygen enters into the respective anode/cathode through the top of the AFC, fills the fuel cell, and any excess gas exits from the bottom into a small chamber filled with water to create a small back pressure that serves to partially scrub the gas of residual KOH carryover. The outlet flowrates are also measured using flowmeters in order to determine the overall gas consumption at each electrode.

A test load cell was connected to the AFC. The current was initially set at 0 A, and increased by 1 A every 5 min. The voltages generated were displayed on the test load screen. Energy captured in the electrical load cell was dissipated in the form of heat through the heat sink situated at the back of the load cell.

Table 1
Summary of the 3 types of tests performed: effect of temperature, KOH concentration and gas flowrates on AFC performance

	Temperature (°C)	KOH concentration (M)	Gas flowrates (mL min^{-1})
1	40, 50, 60, 70	8	Theor O_2 × 3 + 100, Theor H_2 × 6 + 200
2	70	5, 6, 7, 8	Theor O_2 × 3 + 100, Theor H_2 × 6 + 200
3	70	8	Theor O_2 × 3 + 100, Theor H_2 × 6 + 200, Theor O_2 × 1.5 + 50, Theor H_2 × 3 + 100

Table 1 summarizes the three types of tests that were done to test the effect of temperature, KOH concentration and gas flowrates on performance. For each test the temperature, KOH concentration and gas flowrates were varied individually, keeping the other two variables constant.

3. Results

3.1. AFC operating characteristics

3.1.1. Effect of operating temperature

The fuel cell performance was measured as a function of temperature over the range of 40 °C to 70 °C. From the polarization curve in Fig. 2, it was found that as temperature increases, the overvoltage decreases. For any given current, as the temperature increases, the voltage output increases. With an increase in temperature, the power output also increases due to the improved reaction kinetics. There is a decrease in the ohmic polarization because of the increased conductivity of the electrolyte at higher temperatures. At the same time the activation polarization also decreases because of improved kinetics at higher temperature. The contributions to the change in current/voltage behaviour can be determined if one considers the total polarization of the electrode to be given by expression (1):

$$\eta_{\text{total}} = \frac{2.303\,RT}{\alpha z F}\log\left(\frac{i}{i_o}\right) - \frac{2.303\,RT}{\alpha z F}\log\left(1-\frac{i}{i_L}\right) + i\,(R_s + R_f) \quad (1)$$

where i_o is the exchange current density; α the transfer coefficient; z the number of electrons; F the Faraday's constant; R the gas constant; T the temperature; R_S the solution resistance; R_f the film resistance.

Making some basic assumptions (not diffusion limited, not passivated, no change in reaction mechanism/activation step), this can be reduced to expression (2):

$$\eta_{\text{total}} = \frac{2.303\,RT}{\alpha z F}\log\left(\frac{i}{i_o}\right) + iR_s \quad (2)$$

Hence, the activation term has temperature dependence and so does the solution resistance term.

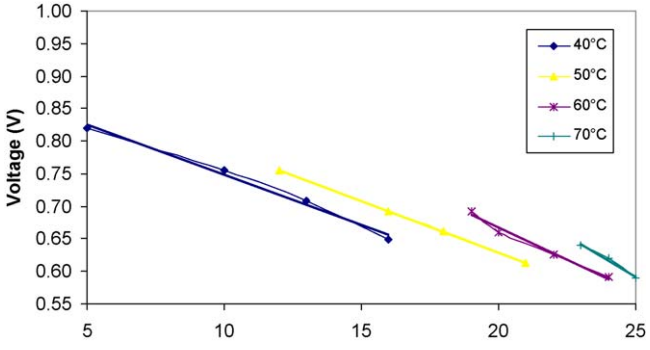

Fig. 2. Effect of temperature on performance–Increasing temperature causes decrease in overvoltage.

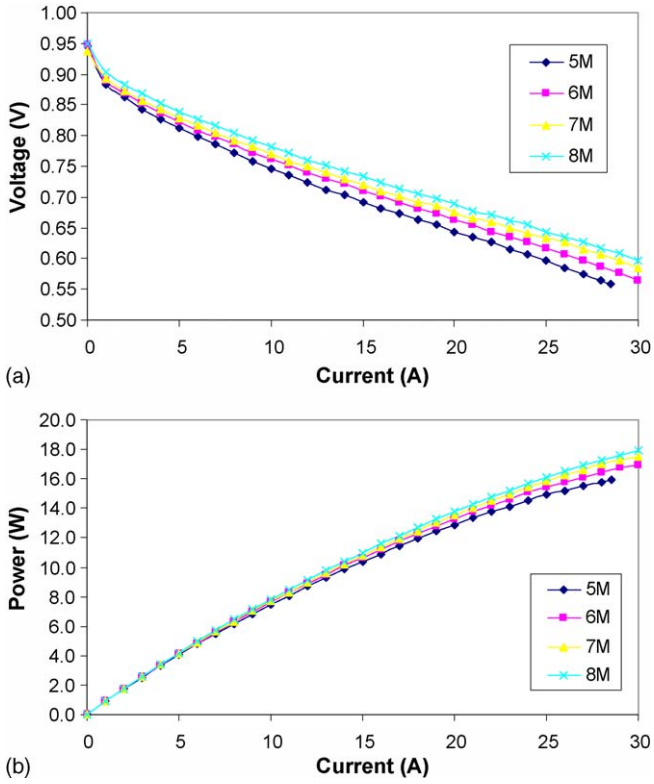

Fig. 3. (a) Effect of concentration on performance—increasing KOH concentration causes a decrease in overvoltage. (b) Effect of concentration on power output—increase KOH concentration causes an increase in power output.

Fig. 2 is an extrapolation of a small range of points. When the electrolyte is fed into the AFC at 70 °C, the actual operating temperature within the fuel cell is not 70 °C. In fact, the operating temperature within the fuel cell is dependent on the amount of current that is drawn from the fuel cell because the fuel cell is a load following device. At currents of 0 A to 12 A, the operating temperature within the cell is 40 to 50 °C. From 12 A to 18 A, the temperature is 50 to 60 °C. For currents of 18 A to 23 A, the temperature is 60 to 70 °C. Finally, for currents of 23 A to 25 A, the temperature within the cell reaches 70 ± 2 °C. Hence, the plots are not complete polarization curves because each portion is extracted according to the AFC (internal) operating temperature. The OCV (open circuit voltage) would otherwise be similar to that of Fig. 3a.

The data plotted in the current–voltage curve are only a small part of the polarization curve and are data that are close to the limiting current for the stack. The limiting current effect is most noticeable for the 70 °C data in which the rate of voltage decline is most rapid. Away from the limiting current, slopes will decrease with temperature, but near the limiting current slopes increase with temperature.

3.1.2. *Effect of electrolyte concentration*

The fuel cell performance was determined as a function of KOH concentration over the range of 5 to 8 M. From the polarization curve in Fig. 3a, an increase in concentration can be seen to decrease the polarization. Fig. 3b is a plot of power versus current for different concentrations. At higher concentrations, there

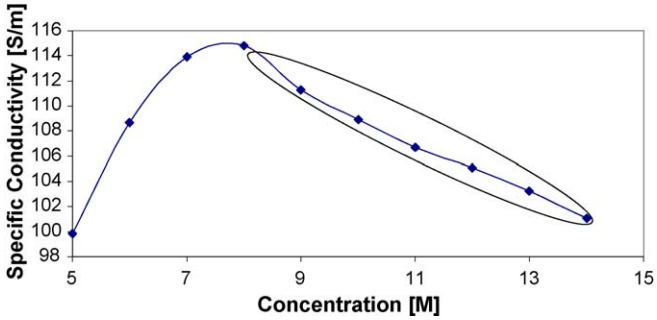

Fig. 4. Graphical representation of the specific conductivity of KOH solutions at 60 °C [5]. Maximum specific conductivity obtained at 8M KOH.

are more OH^- ions available for conduction. The conductivity of the solution increases; hence, the electrolyte resistance within the cell decreases causing a decrease in voltage loss at a constant current ($V = IR$). Since power is the product of current and voltage, the power increases with increasing KOH concentration up to 8 M.

For most solutions, conductivity is proportional to its ion concentration [4]. For some highly concentrated solutions, conductivities can decrease when a certain concentration is reached. This is the case for KOH solutions. Fig. 4 shows a plot of specific conductivity versus concentration for KOH solutions. At concentrations greater than 8 M, the specific conductivity of KOH decreases because the solvation of the K^+ ions at these high concentrations significantly impacts the amount of unbound H_2O molecules in the solution [5]. This causes an increase in electrolyte viscosity and resistance. To minimize bulk cell resistivity effects, KOH concentrations greater than 8 M are not used. At higher KOH concentrations, pore blockage from KOH and K_2CO_3 precipitation has also been observed to limit gas diffusion to active sites and increase cell resistance [6].

3.1.2.1. Resistance. One of the major contributions to overpotential is overall cell resistance. Numerous factors throughout the fuel cell contribute to the observed overall cell resistance:

- Charge transfer resistance occurs on the electrode surface and throughout the electrodes
- Gas diffusion layer (GDL) resistance occurs at the separator/GDL interface
- Hardware resistance occurs in the wires, and contacts
- Electrolyte resistance occurs in the KOH solution

The electrolyte resistivity is the inverse of electrolyte conductivity. Electrolyte conductance at each concentration was obtained by multiplying the specific conductivities of KOH solutions by the cell geometry (area and path length) of the conducting species (electrolyte). Taking the inverse gives us the resistance. From Table 2, it can be seen that as concentration increases, the electrolyte resistance decreases.

The thermodynamic voltage was calculated to be 1.19 V at 70 °C [7]. At open circuit voltage, the voltage for one cell was 950 mV, which indicates a 240 mV drop due to activation irre-

Table 2
Resistivities of KOH solutions at different concentrations at a constant temperature of 60 °C

Concentration (M)	Specific conductivity (at 60 °C), σ (S/m)	Conductivity[a] $C = \sigma A/l$	Resistivity $R = 1/C$ (mΩ)
5	99.85	1997.00	0.500
6	108.68	2173.66	0.460
7	113.93	2278.62	0.439
8	114.83	2296.53	0.435

[a] $A = 0.02\ m^2$, $l = 0.001$ m.

versible losses. This is quite significant compared to the voltage losses associated with the resistances in the fuel cell, since the overall resistance in the AFC ranges from 10.6 to 9.3 mΩ for KOH concentrations of 5 to 8 M, respectively. The deviation from the theoretical voltage is caused by irreversible losses due to the high resistance created by the electrode structure preventing H_2 and O_2 gases from reaching the reaction sites. There may also have been gas crossover because H_2 to O_2 consumption ratio was 2:1.

The hardware resistance made the largest resistance contribution. A breakdown of the hardware resistance into 4 components: tabs, Ni mesh current collector, connector, and wires are shown in Fig. 5. The overall hardware resistance was found to be $5.8 \times 10^{-3}\ \Omega$. Individual component resistances were calculated and the individual cell resistances for the tabs, connector and wires make up about $2.6 \times 10^{-5}\ \Omega$, $2.0 \times 10^{-4}\ \Omega$ and $4.90 \times 10^{-3}\ \Omega$, respectively. The remaining resistance ($6.7 \times 10^{-4}\ \Omega$) is the contribution of the contacts and Ni mesh current collector. The 8-gage wires had the highest contribution to the overall resistance because of the long wires with small cross-sections, and the imperfections in the wires that impede the flow of the electrons, since it is harder to push charge through the wire. The Ni mesh current collector had the second highest resistance because the current that is collected across the nickel mesh current collector embedded within the electrodes has to come out from the small tab located at the edge of the electrodes.

The overall resistance was measured by taking the slope of each voltage-current curve at each concentration. The hardware resistance was found to have the largest contribution, followed by 'other' consisting of resistances from charge transfer, gas bubbles, and GDL/separators also making substantial contribution to the overall resistance. The 'other' resistance was calculated by subtracting the hardware and electrolyte resistance from the overall resistance.

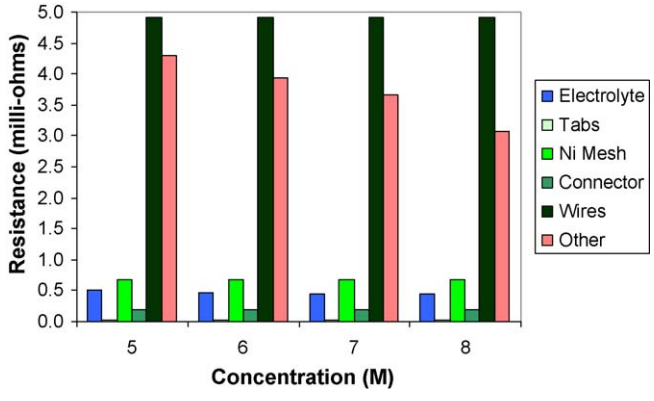

Fig. 5. Overall resistivity broken down into 3 main components: electrolyte, hardware (tabs, Ni mesh, connector and wires), and other.

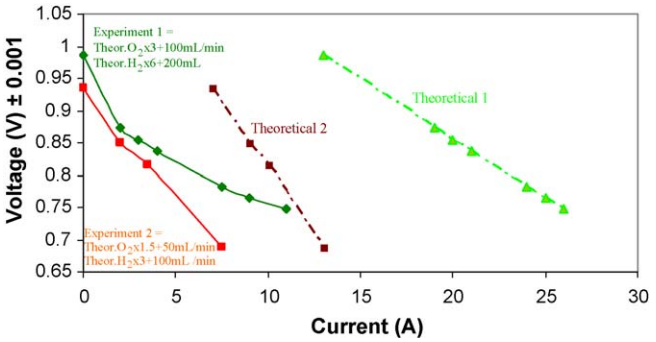

Fig. 6. Effect of gas flowrates on performance—AFC needs at least 6 times the theoretical H_2 flowrate and 3 times the theoretical O_2 in order to operate well.

3.1.3. Effect of gas flowrates

The fuel cell performance was tested as a function of gas flowrate. The theoretical amount of gas needed to produce current was calculated using Faraday's Law. By subtracting the voltage loss from the ideal voltage, and plotting this difference against the current allowed the plot of the theoretical voltage in the polarization curves in Fig. 6.

For example,

$$\text{voltage plotted} = \text{ideal voltage} - \text{voltage loss} = 1.229 - IR$$

$I = 0, 1, 2, 3$ A; $R = 0.0186\ \Omega$ (determined experimentally).

To produce a steady state output current of 20 A at 70 °C, input reactant gas flows of ca 167 mL min^{-1} of H_2 gas and 83 mL min^{-1} of O_2 are required. The AFC would not start or exhibit stable performance when these theoretical flowrates were used. Instead, the amount of gases that was actually required experimentally is approximately 6 times the theoretical of H_2 flowrate and 3 times the theoretical of O_2 flowrate with some additional initial flow; determined through trial and error experiments. Two tests were conducted and the results are plotted in Fig. 6:

- Experiment 1: theoretical O_2 flow times 3 + 100 mL min^{-1}, and theoretical H_2 times 6 + 200 mL min^{-1}
- Experiment 2: theoretical O_2 flow times 1.5 + 50 mL min^{-1}, and theoretical H_2 times 3 + 100 mL min^{-1}

At a set current the gases were initially fed with experiment 1 flowrates for 5 min, and then the gases were decreased by 50% to experiment 2 flowrates for a period of 5 min. The current was increased by 1 A (every 10 min), and the gas flowrates changed back to experiment 1 flowrates for 5 min, and then changed to experiment 2 flowrates for another 5 min. The voltage output was recorded.

The theoretical voltages were calculated using the experimental resistances at each flowrate ($V = IR$). Since the resistance between experiment 1 and 2 were different, the slopes of the theoretical polarization curves at each flowrate were also different. At constant gas flowrates and pressures, the polarization curve should yield the same curves with the same slope.

From Fig. 6 it was found that the fuel cell needs at least 6 times the theoretical H_2 flowrate and 3 times the theoretical O_2 in order to operate well. At a constant voltage of 0.750 V, 11 A is produced using the gas flowrates in experiment 1. Theoretically, at that flowrate, the amount of current that should be produced is 26 A.

Cutting the flowrate by half in experiment 2, it was found that at the same voltage of 0.750 V, 5.5 A of current is produced. Theoretically, 12 A should be produced with the flowrates used in experiment 2. These results indicate that an initial flow is needed to overcome resistances and overvoltages that exist within the fuel cell. Excess gas is needed to ensure that there is gas delivery to the electrode reaction sites where a catalyst is present. Gases need to find a reaction site, which indicate that catalysts are poorly distributed in this cell. Evidence of this will be shown in Section 3.3. Any excess gas that does not find a reaction site leaves the system. By cutting the gas flowrates by half, the cell undergoes higher polarization. At higher currents, the cell experiences starvation. It may be concluded that the gas diffusion layer (GDL) in this fuel cell is inefficient.

3.1.3.1. Actual gas consumption. To determine the actual fuel consumption, the flowrate out was subtracted from the flowrate in. One must also remember that some of the gases that were not consumed could have been lost through crossovers. From this, it was found that the anode electrodes used more H_2 gas at low currents and less H_2 gas at high currents relative to the experiment1 flowrates set at (Theoretical $H_2 \times 6 + 200\,mL\,min^{-1}$). From Fig. 7, 3 trial experiments were conducted and analyzed. The anode electrode had uneven H_2 consumption rates at low and high currents. The curves possessed 3 different slopes. Since the water forms at the anode, the water generated through the reactions may hinder the diffusion of the H_2 to the reaction sites or even block the reaction sites. There were a substantial amount of KOH and water leaving the system through the gas streams, which indicates that the GDE (gas diffusion electrode)

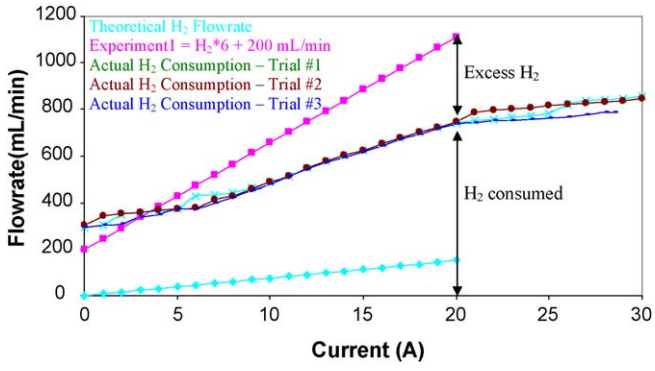

Fig. 7. Anode electrodes used more H_2 gas at low currents and less H_2 gas at high currents shown in the curves with 3 different slopes.

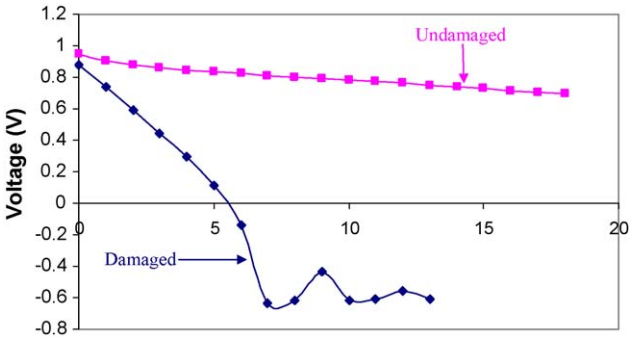

Fig. 8. Polarization curve of a damaged cell vs. undamaged cell.

in the anode side is poorly built. Thus, water and electrolyte consistently entered the hydrophobic area of the GDE. This phenomenon is known as weeping, and it is due to the instability of the PTFE in the GDE. The wet hydrophobic layer will obstruct the gases' pathway to appropriate reaction sites.

3.2. AFC electrode degradation

Two forms of "electrode failures" were encountered while studying the operating characteristics of the AFC:

- Overheating at the anode electrode caused by poor microfluidics within the fuel cell.
- Overpressure at the cathode electrode caused by the overpressurizing of oxygen gas during purging.

The polarization curve for a damaged cell undergoes much higher polarization compared to the undamaged cell (Fig. 8). The potentials measured become negative, and instead of producing electrons, the AFC is actually consuming electrons by reducing the oxide films on the electrode or electrocatalysts causing further damage to the system.

Eleven percent of the electrode surface was damaged (22 cm^2 of the 200 cm^2 total active area). Hence the cell operated at positive potentials up to 6 A before the potentials were inverted. After inverting, the voltage remained negative and independent of current because the current that should be collected escapes through the damaged area causing an increase in resistance.

3.2.1. Anode failure

Forensic examination of the fuel cell revealed that the gas diffusion layer and the active layer were physically attached to the scrim/mesh separator (Fig. 9a). From the optical micrographs, the active layer underwent spalling (Fig. 9b and c). The area around the spall shows the grids of the scrim/mesh separator being thermally deformed as evident by a change in cross-section and alignment of the grid fibres.

The scrim consists of a weave of two fibres that differ only in their nominal thickness. Two samples were taken from the scrim separator, one from the damaged area, and the other from the undamaged area. The relative change in the grid size is summarized in Table 3.

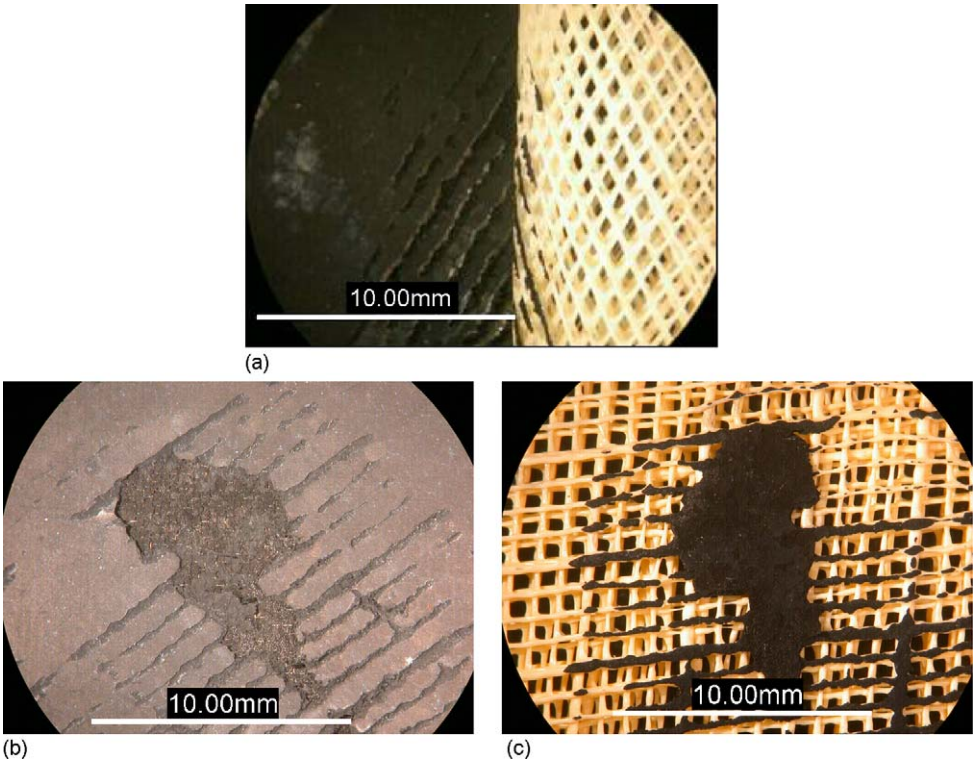

Fig. 9. (a) Optical picture of anode electrode physically attached to the separator. (b, c) Optical pictures of anode active layer undergoing spalling.

Table 3
Change in grid size for undamaged and damaged separator

	Undamaged		Damaged	
	Thick	Thin	Thick	Thin
Maximum (mm)	0.50	0.32	0.47	0.41
Minimum (mm)	0.42	0.28	0.33	0.20

From the results, it shows that the grid strands in the undamaged sample varies from the range of 0.42 to 0.50 mm for the thick strands, and 0.28 to 0.32 mm for the thin strands. For the damaged sample, the grid strands vary much more severely, with the thick strands ranging from 0.33 to 0.47 mm, and the thin strands from 0.20 to 0.41 mm.

The greater variation in separator mesh dimensions in the damaged sample is indicative of the extent of thermal deformation of the fibres. The separator mesh was identified as polyvinylchloride (PVC), and its flow temperature is ∼80 °C [8]. Poor microfluidics within the fuel cell resulted in incomplete flooding with electrolyte (KOH) when hydrogen was injected allowing the internal local temperature to exceed 80 °C. As a result, the separator mesh flowed thermally and bonded to the electrode structure damaging both the electrode and the separator mesh.

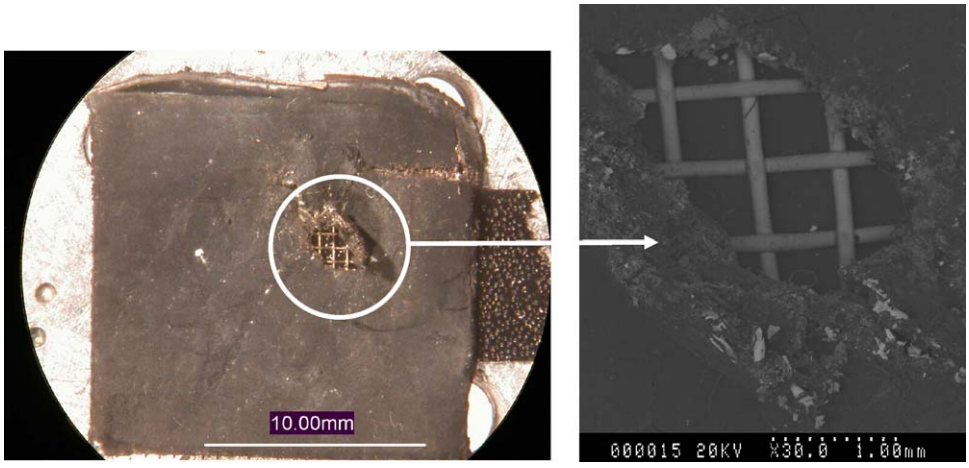

Fig. 10. Cathode perforation due to oxygen gas overpressure.

3.2.2. Cathode failure

A second failure was observed on the cathode. Evidence was seen first with excess leakage of KOH electrolyte into the O_2 gas outlet stream. Forensic investigation revealed a perforation of the cathode electrode caused by excess oxygen gas pressure during purging as seen in Fig. 10. This resulted in complete disbonding between the Ni screen and electrode structure. This will cause charge transfer and hardware resistances to increase drastically because the electrode material and the current collector are no longer in contact.

3.3. Performance degradation

The performance of an AFC is dependent on many factors. The effect of different operating characteristics on performance has been examined. What other factors cause one cell to polarize more than others? Looking at the microscopic level, the catalysts used in this AFC were investigated.

3.3.1. Catalyst distribution

It appears that the electrodes were fabricated using the dry method of rolling the catalyst mixtures with the electrode materials because the catalyst particles on and within the electrodes appeared to be flake-like in shape with a series of dendrites with an interdendritic region that acts as pores.

PdAgCu solid solutions as catalysts were randomly distributed on the anode electrode surface. From the SEM/EDS analysis (Fig. 11), the catalysts were all in the micron-size range. Fig. 12 shows the size distribution obtained through image analysis of a cluster of 486 PdAgCu catalysts making up 20.3% of the total area. The catalyst loading for the anode electrode was

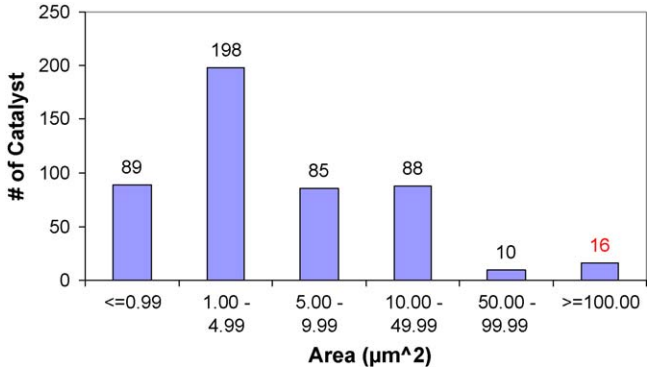

Fig. 12. Size distribution of PdAgCu catalysts on the anode electrode.

1.28 mg cm^{-2} (Pd: 0.70 mg cm^{-2}, Ag: 0.11 mg cm^{-2}, and Cu: 0.47 mg cm^{-2}).

Predominantly Ag particles were found distributed on the cathode electrode surface (Fig. 13). The size distribution of the catalysts on the cathode appeared to be larger than the catalysts used on the anode. Fig. 14 shows the size distribution for the surface cathode catalysts. An SEM micrograph of the cathode electrode surface found 227 Ag particles on the surface making up 1.89% of the total area. The catalyst loading for the cathode electrode with Ag particles on them was 0.0396 mg cm^{-2}. This surface catalyst loading is low relative to commonly reported catalyst loadings but because the reactions occur within the active layer where the three-phase zone is present, the surface loading is not critical. The catalyst loading for the catalysts embedded in the cathode electrode was 0.748 mg cm^{-2}.

The catalysts would be of better use if they were all in the nano-size range. A large amount of catalysts with sizes >100 µm^2 (for the anode), and >10,000 µm^2 (for the cathode)

Fig. 11. Large PdAgCu solid solution catalyst found on the anode electrode.

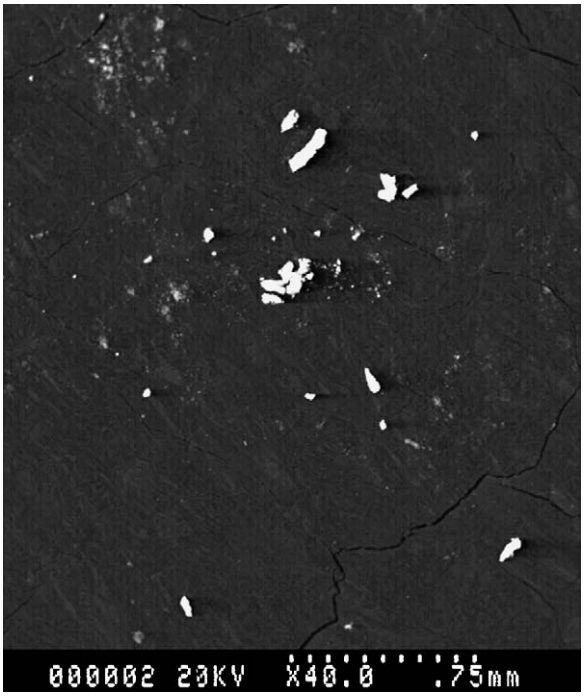

Fig. 13. Large Ag particles found on the cathode electrode as catalysts.

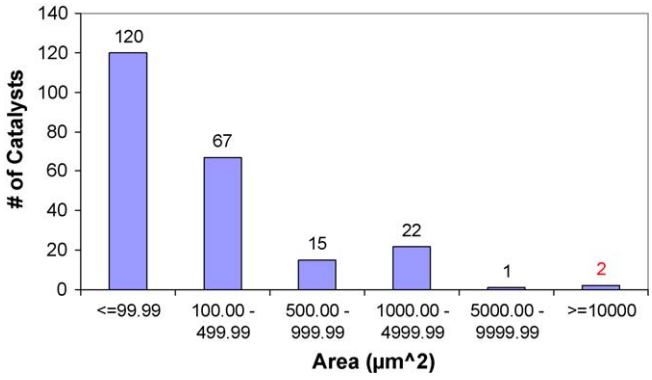

Fig. 14. Size distribution of Ag surface catalysts on the cathode electrode.

were found. The chances of gases finding reaction sites would increase if these large catalysts were crushed into smaller nanopowders.

3.3.2. Catalyst chemistry

The catalysts found on the surface and within the electrode structure were examined. The sizes of the catalysts ranged in the 10–100s microns. From the SEM picture of the perforated cathode, different types of catalyst combinations were found along the mouth of the perforations. From the EDS analysis, they were identified as Ag particles, AgMn, and PdCuMn solid solutions (Fig. 15).

Examining the effects of the catalysts on performance, it was found that:

- There is poor control of catalyst chemistry in this AFC, because different types of catalysts were scattered on and within the electrode structure.
- There is poor control of catalyst distribution as evident by the large size of the catalysts leading to micron, and not nanometer size distributions observed in other fuel cell systems.
- These two factors lead to poor catalyst utilization making it difficult for gases to find suitable number and chemistry of reaction sites, hence, the inconsistent performance of the cells.

The catalysts used in this AFC were large in size distribution and had chemistry not ideally suited as electrocatalysts. The usage of large catalyst sizes (in the micron-size range) hinders the performance of the AFC. Therefore, having catalysts with sizes in the nano-range will allow better use of the specific surface area of the catalysts and reduce costs per unit power produced. Poor chemistry due to the random mixture and dispersion of materials to make up the supported catalysts leads to a condition of non-ideal loading where a significant fraction of the material added may be either inert, non-catalytic or may promote undesirable side reactions. Thereby optimizing a composition that is known to be electrocatalytic for one or more of

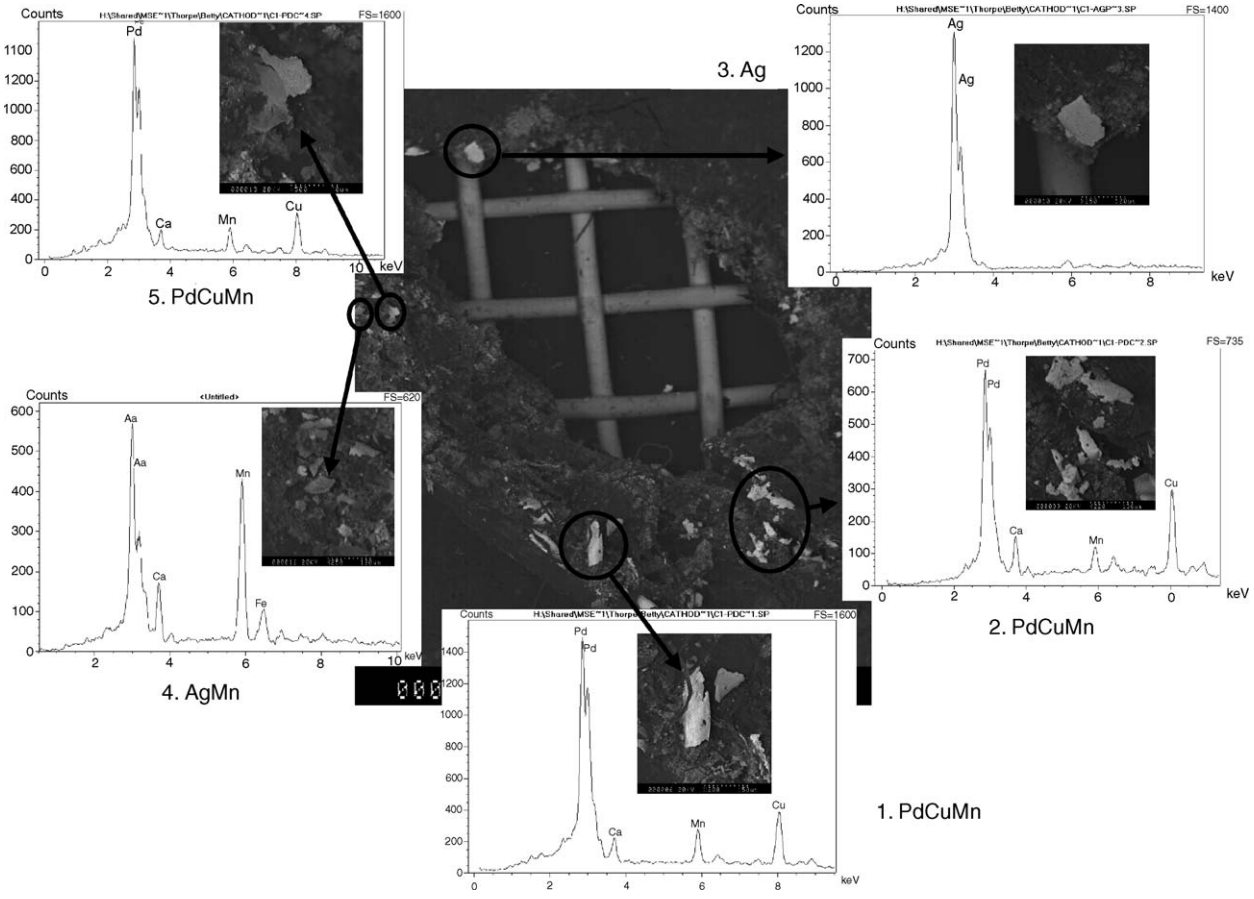

Fig. 15. Different types of catalysts (Ag particles, AgMn, and PdCuMn solid solutions) found within the cathode electrode.

Table 4
Possible replacements for existing materials in an AFC

Component	Existing material	Limitations to existing material	Proposed change
End plates	Plexiglass	Temperature/strength	PPO or PPS
Frame	Epoxy	Temperature	PPO or PPS
Separator	PVC	Low flow temperature	Teflon
Current collector	Ni mesh	Bonding to carbon	Perforated Ni Foil
Gas diffusion layer	Carbon, PTFE		
Active layer	Carbon, PTFE, catalysts		
Anode catalyst	Micron-size PdAgCu	Expensive, large catalyst size	Nano-size Raney Ni powder
Cathode catalyst	Micron-size Ag, AgMn, PdCuMn	Poor chemistry, large catalyst size	Nano-size Ag powder
Connectors	Small diameter	High resistance	Use busbars to increase cross-sectional area
Electrode design	Flat surface, no flow channels	Non-uniform electrolyte distribution	Add electrolyte flow channels
System design	Use of 'glue' and gasket to seal the electrodes together	Electrolyte leakage	Injection moulding

the reaction steps involved, and suitably dispersing these in a conductive supporting medium on a nanoscale, improved gas utilizations are expected.

4. Future considerations

Materials that can be used to improve the AFC are shown in Table 4.

5. Conclusion

It was found that although there are many advantages to the AFC, there are also challenges that need to be overcome in order to advance the AFC technology to the same level as the AWE.

- The AFC stack performance is comparable to the performance reported in the literature for other circulating electrolyte fuel cells. However, the power output is limited by temperature build up in the stack. The stack temperature limit should be set at 70 °C maximum to avoid damaging the cell components. Improvements in microfluidics and electrolyte management are needed to allow higher power output and to ensure more uniform thermal profiles within the AFC.
- The AFC performance increased with concentration from 5 to 8 M. Due to higher electrolyte concentration resistances, the electrolyte concentration should be kept ∼8 M to obtain optimum ionic conductivity. Other than the irreversible losses at open circuit voltage, hardware resistances made the largest contribution to the overall resistance.
- Excess gas is needed to ensure that there is gas delivery to the electrode reaction sites where a catalyst is present. Gases need to find a reaction site, which indicate that catalysts are poorly distributed in the AFC. Unstable performance occurred when the hydrogen gas supply becomes limiting due to water management problems in the anode electrode.

Investigating the two mechanisms of failure highlighted needed improvements in cell design and materials in the AFC:

- Improvements in microfluidics and electrolyte management are needed to ensure correct thermal profiles within the AFC to avoid damaging the cell components.
- Improvements in performance can be achieved by better catalyst formation, chemistry, and size distribution and utilization.

References

[1] M.L. Perry, T.F. Fuller, J. Electrochem. Soc. 149 (2002) S60.
[2] K. Kordesch, G. Simader, Fuel Cells and their Applications, Wiley, New York, 1996, p. 58.
[3] K. Kordesch, G. Simader, Fuel Cells and their Applications, Wiley, New York, 1996, p. 61.
[4] S.H. Lee, Bull. Korean Chem. Soc. 22 (2001) 847.
[5] G.G. Aseyev, I.D. Zaytsev, Prop. Aqueous Solutions Electrolytes (1992) 794.
[6] P. Gouerec, L. Poletto, J. Denizot, E. Sanchez-Cortezon, J.H. Miners, The evolution of alkaline fuel cells with circulating electrolyte, J. Power Sources 129 (2004) 193–201.
[7] R.L. LeRoy, Int. J. Hydrogen Energy 8 (1982) 401.
[8] C.A. Harper, Handbook of Plastics and Elastomers, McGraw-Hill Inc, New York, 1975, 1–67.